Characterization of seabed properties from Scholte waves acquired on floating ice on shallow water

Tor Arne Johansen[1,2,3*] and Bent Ole Ruud[1,2]

[1]*Department of Earth Science, University of Bergen, Bergen, Norway,* [2]*ARCEx, Research Centre for Arctic Petroleum Exploration, University of Tromsø, Tromsø, Norway, and* [3]*The University Centre in Svalbard, Longyearbyen, Norway*

ABSTRACT

Seismic surveying of the coastal areas in the Arctic is best facilitated during wintertime when the sea ice is land-fast. This eases the logistics of the operation and assures that there is no damage made to the vulnerable tundra. Seismic experiments on floating ice on shallow water performed in a fjord in Svalbard in the Norwegian Arctic show prominent Scholte waves. The dispersion relation of Scholte waves can provide the shear wave velocities of the seabed sediments. Scholte wave data can potentially be obtained when the seismic source and geophone receivers are both placed on top of the floating ice. However, the Scholte wave data become more distinct by using an air gun lowered some metres below the ice. A rock physics model based on a two-step differential effective medium scheme has been tuned to predict seismic properties found for very loose sediments, among these very high P-wave to S-wave velocity ratios. The rock physics model enables us to convert seismic velocities obtained from Scholte wave data to quantitative estimates of the sediment composition.

Key words: Data acquisition, Inversion, Modelling, Shallow marine, Surface wave.

INTRODUCTION

The architecture and composition of sediments in the near coastal areas of the Arctic may reveal the most recent geological processes and climate history. Geological processes caused by retreating or advancing glaciers lead to alternating erosion, melt-water flux and sedimentation rates. Echo sounding and sediment coring can provide sediment morphology and near-surface layering. Due to the sea ice dynamics in these coastal areas, access to various field sites is often best during wintertime when the sea or fjord ice is land-fast. Seismic data can provide estimates of *in situ* mechanical properties of the seabed sediments (Vardy *et al.* 2017). Reflection and refraction data can provide mechanical properties in case of deep water. At shallow water, guided wave modes along the seabed can provide similar information. Two types of guided waves along the seabed may occur, referred to as Leaky Rayleigh and Scholte waves. Many authors, among them Bohlen *et al.* (2004), Kugler *et al.* (2005, 2007), Park *et al.* (2005) and

Boiero, Wiarda and Vermeer (2013), have demonstrated the use of Scholte waves for evaluating the mechanical strength of the seabed. Such properties depend on the geological processes at the time of sediment deposition and the subsequent mechanical compaction. In geological terms, this influences sediment composition, porosity and granular structure, as sorting along with shape and roughness of grains.

During the winter season of 2016 several seismic experiments were conducted on floating ice in the inner part of Van Mijenfjorden in the Norwegian Arctic. Figure 1 shows the field location. The aim of the study was to unravel the complex wave field recorded on and below floating ice on shallow water. The seismic source was a single air gun deployed in water below the ice or explosives (detonating cord) placed at the surface of the ice. The seismic receivers were strings of gimballed geophones placed on the ice, three-component (3C) geophones on the ice, hydrophones lowered to various depths below the ice, and four-component ocean bottom nodes deployed at the seabed.

Results from experiments on floating ice conducted by Johansen, Ruud and Hope (2019a,b) show that guided waves

*E-mail: torarne.johansen@uib.no

Figure 1 Map over study area. The data were acquired along the red line in March 2016.

along the seabed referred to as Scholte waves can be generated either using an explosive source at the surface of the ice or using an air gun below when the water depth is relative shallow.

In this paper, we analyse Scholte waves obtained from seismic data acquired on floating ice and discuss how they can provide quantitative parameters describing the seabed sediments.

SCHOLTE WAVE DATA ACQUIRED ON SHALLOW WATER

Along the seabed, an interface separating a fluid and a solid, two types of guided waves may exist. These are referred to as Leaky Rayleigh and Scholte waves. While Scholte waves may always exist, Leaky Rayleigh waves may only occur when the S-wave velocity of the seabed (V_s) is larger than the acoustic velocity of water (V_w). In our experiments, the upper seabed sediments are very loose which implies that $V_s << V_w$ and we need only to consider Scholte waves. By considering the fluid and solid as two half-spaces, the Scholte-wave velocity V_{Sc} is found from Vinh (2013):

$$rx^2\sqrt{1-\beta x} + (2-x)^2\sqrt{1-\beta^* x}$$
$$-4\sqrt{1-x}\sqrt{1-\beta x}\sqrt{1-\beta^* x} = 0, \quad (1)$$

where

$$x = \frac{V_{Sc}^2}{V_S^2}, \quad \beta = \frac{V_S^2}{V_P^2}, \quad \beta^* = \frac{V_S^2}{V_w^2}, \quad r = \frac{\rho}{\rho^*},$$

and where V_p denotes the P-wave velocity of the sediment, and ρ and ρ^* are the densities of water and sediment, respectively. Often $V_{Sc} = 0.9\ V_s$ is a good approximation for the Scholte-wave velocity (Johansen et al. 2019a). When sediment properties and correspondingly seismic velocities vary with depth the Scholte waves become dispersive and several wave modes occur. Scholte waves are generated when a seismic source is fired at or close to the seabed (De Hoop and Van der Hilden 1983; De Hoop and Van der Hilden 1984). However, they may also be triggered from seismic waves incident on a seabed with topography (Zheng et al. 2012).

Our experiments took place on 30–40 cm thick ice floating on shallow water. Figure 2 shows how geophones and hydrophones were placed on ice, in water and at the seabed. Further details about the seismic experiments and the recording equipment can be found in Johansen et al. (2019a,b). The instrument responses were all similar to that of analogue geophones, but with a natural frequency, which varied between the different types of sensors. The geophones of the ocean bottom node (OBN) and the strings with vertical gimbal sensors were both with 14 Hz natural frequency, while the three-component (3C) geophones had a natural frequency of 10 Hz. The hydrophones were of a transformer-coupled type with a frequency response similar to that of a 10 Hz
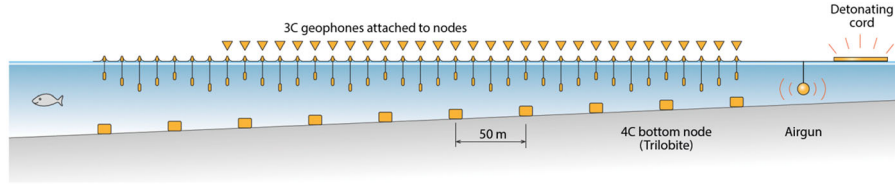
Figure 2 Experimental set-up. Two types of geophones were used at the ice surface: single three-component (3C) 10 Hz geophones and strings with eight vertical, gimballed 14 Hz geophones. Both types of geophones and also the hydrophones, which were deployed at various depths, were connected to RAU-3 Unite nodes (Sercel) for recording. The sea bottom nodes, containing both 3C geophones and hydrophones, were Trilobits from Seabed Geosolutions.

geophone. Before analysis, all recordings were brought to a common natural frequency of 5 Hz by processing. This means that the instrument response were made flat above 5 Hz and that it falls off with a slope of 12 dB/octave below 5 Hz. In addition, the phase response of the different instruments was made identical. This process amplified the energy at frequencies below the natural frequencies, which were of particular interest in this study. Furthermore, the higher frequencies (>15 Hz) were damped or completely removed (>60 Hz) by a low-pass filter. As will be seen, a remarkable property of the Scholte waves observed in this study is the narrow bandwidth from 3 to 5 Hz. This is not a result of the recording or processing, but it is due to the properties of the seabed sediments.

Scholte waves are evanescent waves with amplitudes decaying exponentially with distance from the seabed. Furthermore, at shallow water the resulting amplitudes are modulated by interference of the surface. When seismic waves in a stack of horizontal layers are analysed in terms of angular frequency $\omega = 2\pi f$ and horizontal slowness p, there are four types of waves in an isotropic solid layer: upward and downward propagating P and S waves (here we have left out the SH waves which do not couple to the P and SV waves). For a model with a water layer at the top, only the two P waves can exist, and consequently the analysis of the waves in the water layer becomes much simpler. The pressure P is the sum of the pressures associated with the two waves:

$$P = P_d + P_u \tag{2}$$

and (in two-dimensions spanned by the x- and z-axes with the z-axis pointing downward) the pressure of these waves is given by

$$P_{d/u} = A_{d/u} \exp\left[i\omega\left(px \pm \xi z - t\right)\right] \tag{3}$$

where t is time and $\xi = \sqrt{V_w^{-2} - p^2}$ is the vertical slowness. From the surface condition: $P = 0$ at $z = 0$, we find that the amplitudes of the two waves must satisfy $A_u = -A_d$.

Since the S-wave velocity here is much less than the P-wave velocity in water, ξ will be complex. For $p \gg 1/V_w$, it can be approximated by $\xi = ip$. Then the pressure can be written as

$$P = A_d \left[\exp\left(-\omega p z\right) - \exp\left(\omega p z\right)\right] \exp\left[i\omega\left(px - t\right)\right]. \tag{4}$$

The total pressure is the sum of the pressure from two evanescent waves, one decaying downward and one decaying upward. We see that the amplitudes of the pressure waves vary with depth according to the terms $\exp(\pm\omega p z)$. In analogy with electromagnetic waves, we define a 'skin depth' $\delta = (\omega p)^{-1}$ for an evanescent wave as the depth where the amplitude of the wave is reduced by a factor $e^{-1} \approx 0.37$. For instance, for a Scholte wave with a frequency of 4 Hz and a phase velocity of 100 m/s, the skin depth is about 4 m. This means that for a Scholte wave at deep water, the amplitude (pressure or some other quantity like displacement or particle velocity) will decay exponentially upwards and it will be reduced to 37% of the amplitude at the seabed, 4 m above the seabed. For shallow water, the situation will be different because we must also take the 'surface reflection' (the wave with amplitude decreasing with depth) into account.

For an ocean bottom node, the vertical particle velocity is of interest in addition to the pressure. The vertical particle velocity in water can be computed from the pressure (Johansen *et al.* 2019b) as $V_z = (i\omega\rho)^{-1}\frac{\partial P}{\partial z}$. This gives

$$V_z = \frac{\xi}{\rho} A_d \left[\exp\left(i\omega\xi z\right) + \exp\left(-i\omega\xi z\right)\right] \exp\left[i\omega\left(px - t\right)\right] \tag{5}$$

and for Scholte waves with $p \gg 1/V_w$, we get

$$V_z = \frac{ip}{\rho} A_d \left[\exp\left(-\omega p z\right) + \exp\left(\omega p z\right)\right] \exp\left[i\omega\left(px - t\right)\right]. \tag{6}$$

Comparing this to the corresponding expression for the pressure, we note a 90° phase difference between the pressure and the vertical particle velocity for evanescent waves in the water.

In Figure 3, the depth dependence of both the pressures and vertical particle velocity motions are shown as functions of the skin depth. It is seen that for depths less than the skin
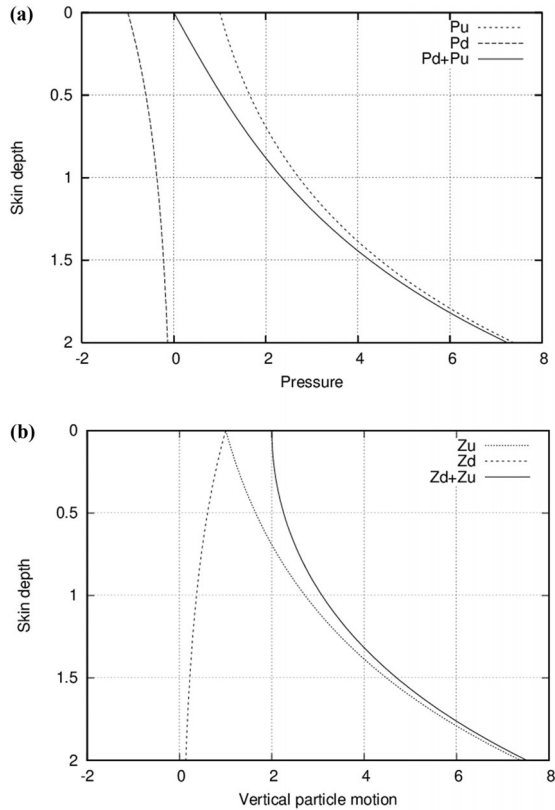
Figure 3 The depth dependence of pressure (a) and particle velocity motion (b) in a water layer are shown as functions of the skin depth for evanescent waves with phase velocity much less than the acoustic velocity in water. The amplitudes are normalized so that the upward decaying waves have amplitude 1.0 at the surface.
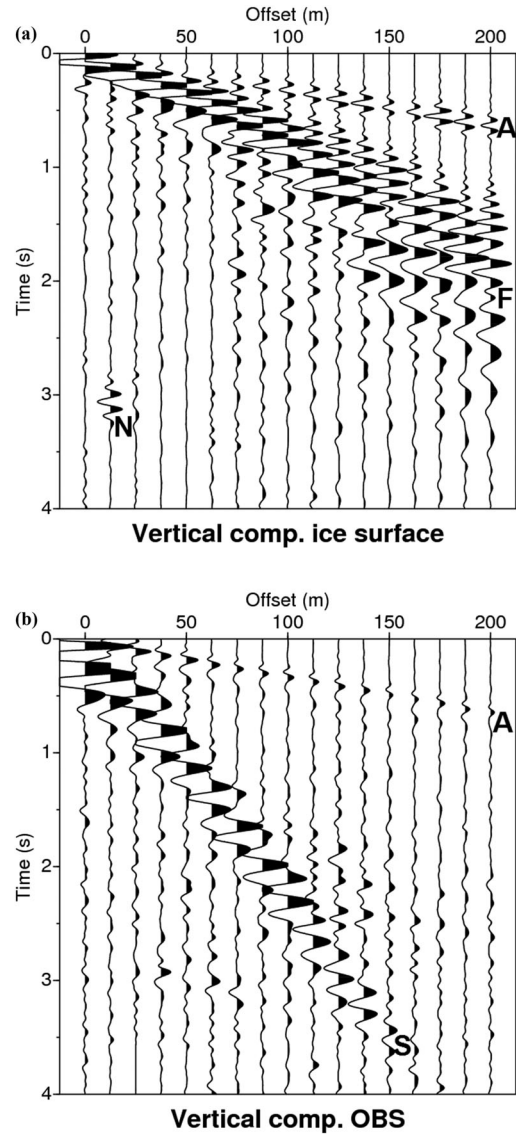

Figure 4 The vertical component of 3C geophone recordings at the top of the ice layer (a) and at the seabed (b). The source is detonating cord (10 m, 0.4 kg explosives) stretched out on the ice surface in the in-line direction. The water depth is about 8 m. At the ice surface, the flexural waves dominate while the Scholte waves dominate at the seabed. Due to the scaling, the first visible arrival here is the air wave, but when plotted with different scaling we find that the first arrivals are other types of waves (propagating in the ice and water layers, and, at larger offsets, refracted P waves propagating below the seabed). (A: air wave, F: flexural wave, S: Scholte wave, N: Noise burst).

depth, the total pressure increases almost linearly with depth, while for depth larger than two times the skin depth, the 'surface reflection' can be ignored and the water layer can be considered as a halfspace with regard to Scholte wave propagation. We also note that the two P waves add constructively for particle motion at the free surface while the pressure waves cancel out. Thus, it is possible to record the Scholte waves with vertical geophones placed at the surface of a thin ice layer, while hydrophones must be deployed deeper into the water layer for Scholte wave recording. For water depths much less than the skin depth, we note that the depth dependence is almost constant. Therefore, a thin water layer (compared to skin depth) can be ignored when considering vertical particle velocity or displacement, and the wave could rather be called a Rayleigh wave. However, one must keep in mind that the skin depth is a frequency-dependent variable (inversely proportional to both frequency and horizontal slowness, which

may also vary with frequency), so that the effect of a water layer will become more noticeable as the frequency increases.

Figure 4 shows common receiver gathers for a string of gimballed geophones resting on top of the floating ice (left), and the vertical displacement component of a four-component
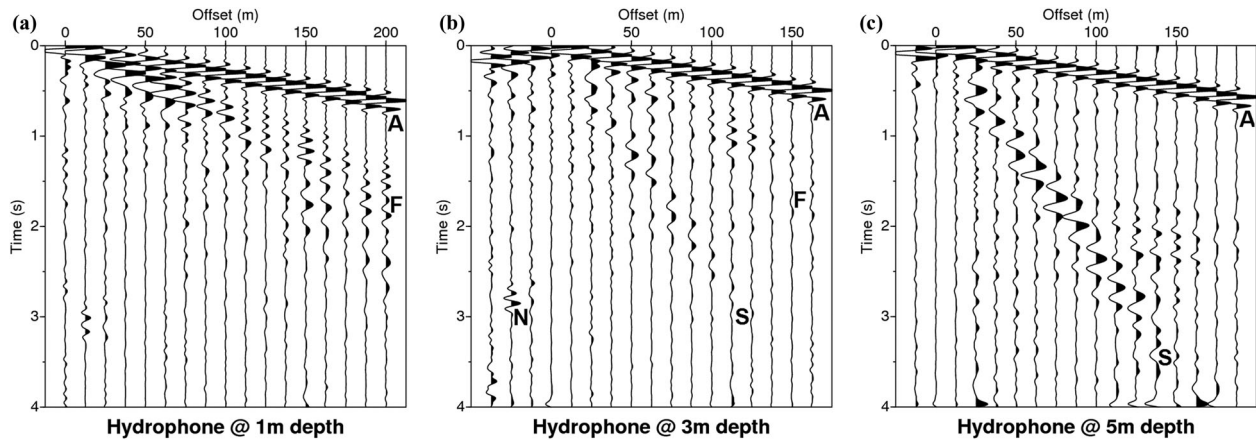
Figure 5 Common receiver gathers recorded by single hydrophones at different depths. The sources were the same as that in Figure 4. We note how the relative amplitudes of the flexural waves and the Scholte waves change with the depth of the hydrophone. (A, air wave; F, flexural wave; N, Noise burst; S, Scholte wave).

node (trilobit) at the seabed (right). The data acquired at the seabed shows a prominent, low frequency, almost monochromatic Scholte wave propagating with a group velocity near 40 m/s. In general, we could expect to see the energy of the surface waves distributed over several wave modes. However, our data do not expose higher order modes most probably because the Scholte wave in our experiment is low frequency dominant. An interesting observation in Figure 4 is that a relatively small amount of detonating cord exploding on floating ice generates a quite energetic Scholte wave. Figure 5 shows similar plots for hydrophone recordings at 1, 3 and 5 m water depths. The effect of the reduced amplitude with increasing distance from the seabed is again obvious and follows the calculations shown in Figure 3.

The use of an air gun below the ice has the immediate advantage of reducing noise from the air wave generated by detonating cord. Figure 6 shows geophone shot gathers at the sea ice using single air gun shots at 1.5 m and 3 m water depths and to the right the corresponding phase velocity versus frequency plots. The phase velocity spectra shows that the main energy lies between 3 and 5 Hz, with its peak energy at about 4 Hz. Considering a phase velocity of about 125 m/s at 4 Hz, the skin depth in the water layer will be 5 m, or the same as the water depth at the source. In view of the analysis related to Figure 3, the amplitude of the Scholte waves from the air gun at 3.0 m should be about twice that of the same source at 1.5 m. The data clearly emphasize an increase in Scholte-wave amplitude and a decrease in ice flexural wave amplitude as the source is displaced closer to the seabed and farther away from the floating ice sheet. Figure 4 reveals how the amplitude of the Scholte wave is reduced on top of the

ice where ice flexural waves dominate. With an air gun, the source can be closer to the seabed and thus more efficiently generate Scholte waves which are now also prominent in the geophone data at the ice surface.

ESTIMATION OF SEABED PROPERTIES

As Scholte waves sample the elastic properties of the near-surface seabed sediments, they can potentially be used to extract sediment properties as porosity and mineral composition. An inversion of Scholte wave data provides an estimate of the S-wave velocity depth profile, which can be used for quantitative sediment characterization based on rock physics. A basic criterion for the success of the inversion is that the S-wave velocity increases with depth, which in our case is true if we neglect any effects caused by the stiff, floating sea ice. Dispersion spectra, as seen in Figure 6, were computed by the slant stack method (McMechan and Yedlin 1981), but with some pre-whitening of the traces. A damped pre-whitening method was applied in order not to severely amplify low amplitude frequencies dominated by noise. The applied method can thus be considered a compromise between the slant stack and the phase shift method of Park, Miller and Xia (1998), in which the trace spectra are completely flattened and only the phase information is retained. Finally, the velocities were picked manually along the branch forming the dominating Scholte wave. Group velocities for various frequencies were estimated by complex trace analysis. The instantaneous frequency (time derivative of the instantaneous phase) was computed for the time interval containing the Scholte wave, and the group velocity was computed from the known travel time and offset.
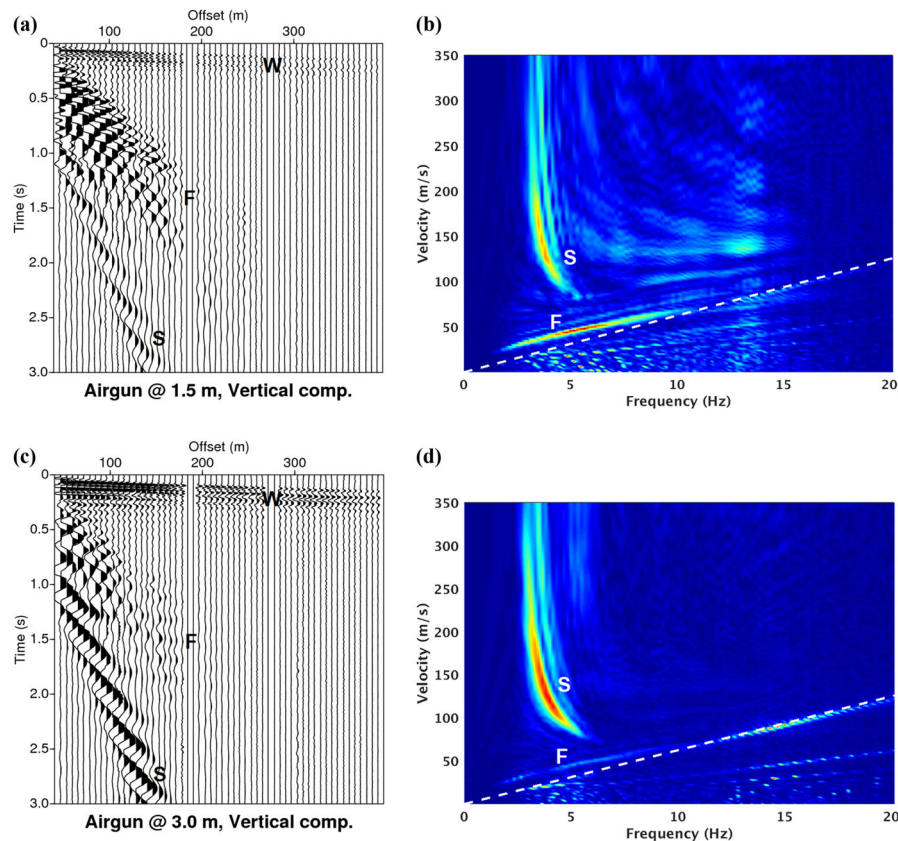
Figure 6 Traces from vertical geophone strings with group length 6.25 m (left) and velocity spectra computed from the same traces (right). The source for these shot gathers was a Mini GI air gun with volume 30 cubic inches deployed at depths of 1.5 m (top) and 3.0 m (bottom). The water depth at the source is about 5 m and about 8 m at the receivers. In both cases, we see both the flexural waves and the Scholte waves, but the flexural waves are weak for the deeper source. The Scholte waves are strongest for frequencies between 3 and 5 Hz and have phase velocities above 80 m/s. The flexural waves are seen for frequencies from 2 to 10 Hz and have phase velocities below 75 Hz. The white dashed line in the velocity spectra indicates the resolution limit due to spatial aliasing. (F, flexural wave; S, Scholte wave; W, water wave).

The group velocities used in the inversion were averaged over several representative receivers. A joint inversion of phase and group velocities was performed by the *surf96* program from 'Computer Programs in Seismology' (Herrmann 2013). Layer thicknesses, P-wave velocities and densities were held fixed in the inversion. The densities were initially assumed to follow the relation between P-wave velocity and density as proposed by Nafe and Drake (Ludwig, Nafe and Drake 1970). In view of the low velocity of the Scholte waves, the P-wave velocities in the sediment layers were set slightly above the P-wave velocity in water. The velocities in the halfspace were based on observed refracted P-wave velocities and an assumed P-wave to S-wave velocity ratio (V_p/V_s) of 1.9. Furthermore, the sediment model was constrained to three layers of constant thicknesses, which was established by trial and error.

The ice layer was ignored in the inversion as the thickness of the ice was much less than the wavelengths involved, and

no interaction between the flexural wave the Scholte wave was observed. As seen in Figure 6, the phase velocity of the flexural wave is about 40 m/s at 4 Hz, giving a skin depth of 1.6 m in the water. This is much less than the water depth, thus there is no noticeable coupling between the flexural wave tied to the ice layer and the Scholte wave tied to the seabed. The phase velocity of the flexural waves may be much higher (for thicker and stiffer ice layers) and the water depth may be less for other surveys, and in such cases the ice layer cannot be ignored when using Scholte wave data.

The model obtained from inversion of the Scholte wave dispersion data is given in Table 2. Figure 7 shows the observed and modelled dispersion data for both group and phase velocities. The model is able to explain both types of observations very well in spite of the large difference between group and phase velocities. Some of the phase velocities are larger than the S-wave velocities in the sediment layers (but
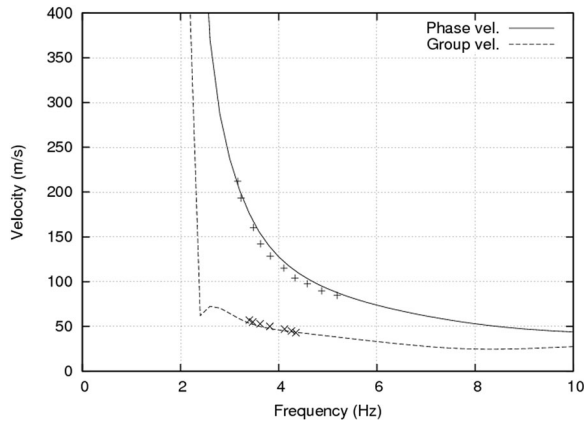
Figure 7 Observed and modelled phase and group velocities. The model, given in Table 2, was obtained by inversion of the observations (shown here as points).

Modelling, Airgun @ 3m, Z-comp.

Figure 8 Synthetic shot gather computed from the inverted model (Table 2). The calculations were performed with the wavenumber integration program OASES (Schmidt 2011). The centre frequency of the source was set to 10 Hz. As there was no ice layer in this modelling, there are no flexural waves. Other waves are very weak due to the low source frequency.

less than the velocity in the water layer and the S-wave velocity of the halfspace) which means that these waves propagate as guided waves in the sediment layers. Thus, the term 'Scholte wave' (which strictly speaking is an evanescent wave at the interface between a liquid and a solid halfspace) can be questioned, but we prefer to keep this name as it is now customary to use for all types of interface and guided waves propagating along the seabed. The S-wave velocity of the lower halfspace did not change in the inversion, which indicates that the observed data could not resolve the velocity at that depth. Furthermore, from the theory of surface waves (Aki and Richards 1980, chapter 7), it is known that the frequency domain amplitude is inversely proportional to both the phase and group velocity. Figure 7 reveals a sharp rise in both the phase and group velocities when going from 3 Hz and towards lower frequencies, which will severely reduce the amplitude below 3 Hz. The almost constant group velocity above 3 Hz will also contribute to a strong time domain amplitude. The absence of energy above 5 Hz is probably due to strong S-wave attenuation in the sediment layer.

The model obtained from the inversion was input to a forward modelling scheme based on a wavenumber integration technique (OASES) as described by Schmidt and Tango (1986). Its usage for modelling guided wave modes is reported in Johansen *et al.* (2019a). Figure 8 shows the synthetic seismograms, and we see that the main characteristics of the Scholte wave are reproduced. A similar modelling experiment using a finite element scheme can be found in Landschultze (2018).

Bachrach, Dvorkin and Nur (2000), Zimmer *et al.* (2007a,b), Walton (1987), Andersen and Johansen (2010) and Moyano *et al.* (2012) have discussed rock physics of under-
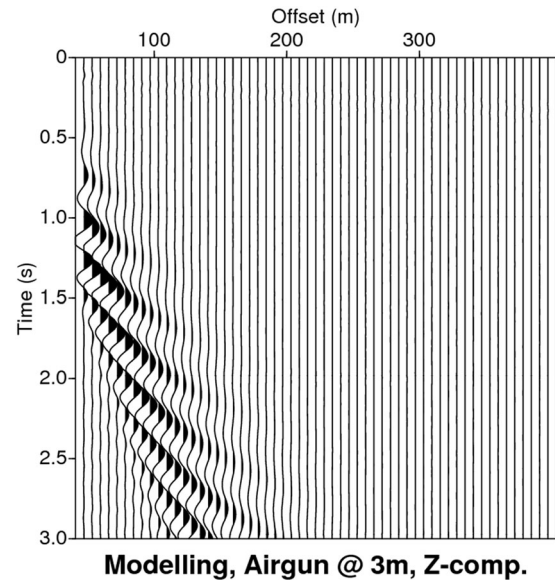
consolidated sediments. However, the vast majority of these models do not apply to very loose, clayey sediments subjected to low effective stress and with porosities close to the suspension limit, often referred to as critical porosity. Hald *et al.* (2001) reported on the composition of sediments in this area. They are recent, loose deposits with a silt-to-clay fraction of about 1. Loose sediments at the seabed may behave like suspensions, with vanishing shear strength as porosity exceeds the critical porosity. In this case, the bulk modulus can be estimated using the equation of Wood (1955). Since Scholte waves are prominent in our data, this is evidence that the sediments hold some shear strength. For estimation of their elastic moduli, we employ a two-step procedure based on a differential effective medium (DEM) scheme, as has been discussed by Berryman (1992). Our modelling strategy assumes that the sediment occurs as a percolated clay–water mix, which embeds silt particles. Below we briefly review the modelling procedure.

The first step is to obtain the elastic properties of a system of connected clay particles in water. The elastic properties of clay and water are given in Table 1. The modelling is initiated from zero porosity clay in which water inclusions of aspect ratio α are embedded. The DEM procedure assures that both clay and water evolve as connected phases as the porosity

Table 1 Physical properties of water, clay and silt used in the modelling

	Bulk (GPa)	Shear (GPa)	Density (kg/m3)	V_p (m/s)	V_s (m/s)
Water	2.165	–	1030	1450	–
Clay	21.0	7.0	2500	3483	1673
Silt	37.0	44.0	2650	6008	4075

Table 2 Layer thicknesses and P-wave velocities were fixed during inversion, and densities were computed from P-wave velocities by the Nafe–Drake relation. Only the S-waves velocities were estimated in the inversion

Layer Number	Thickness (m)	V_p (m/s)	V_s (m/s)	Density (kg/m3)
1	8	1500	–	1000
2	2	1600	44	1217
3	4	1650	95	1478
4	12	1700	168	1645
5	–	4200	2200	2500

increases. The elastic moduli occur from solving the coupled system of ordinary differential equations (Berryman 1992)

$$(1 - y) \frac{d}{dy} [K_{DEM}{}^*(y)] = (K_2 - K_{DEM}{}^*) P^{(*2)}(y) \qquad (7)$$

$$(1 - y) \frac{d}{dy} [\mu_{DEM}{}^*(y)] = (\mu_2 - \mu_{DEM}{}^*) Q^{(*2)}(y), \qquad (8)$$

where y denotes volume fraction of inclusion phase embedded in steps of dy. $K_{DEM}{}^*$ and $\mu_{DEM}{}^*$ are the effective bulk and shear moduli, starting from initial conditions $K_{DEM}{}^*(0) = K_1$ and $\mu_{DEM}{}^*(0) = \mu_1$ which are usually set to the elastic moduli of the initial host material (here clay). K_2 and μ_2 denote the moduli of the added water inclusions and the terms P^* and Q^* are geometrical factors associated with the inclusion material, see Mavko, Mukerji and Dvorkin (1998) for details. Figure 9 shows the elastic properties of a clay–water mix as function of water-filled porosity using various aspect ratios of the inclusion material.

The second step is to include the silt grains which we assume is of spherical shape ($\alpha = 1$). Now, the initial parameters $K_{DEM}{}^*(0) = K_1$ and $\mu_{DEM}{}^*(0) = \mu_1$ are those of a clay–water mix while K_2 and μ_2 are the bulk and shear moduli of silt. Shallow clay deposits may have a porosity in the range of 0.6–0.8 (Avseth, Mukerji and Mavko 2005). By trial and error, we set the clay aspect ratio to 1/30 which gives an S-wave velocity of ca. 10 m/s for a water-filled porosity of 80%. This was done in order to calibrate the modelled S-wave velocities to sediment composition and properties found by Ayres and Theilen (1999) and Hald *et al.* (2001), so that S-wave velocities can be used to estimate seabed properties from the Scholte wave
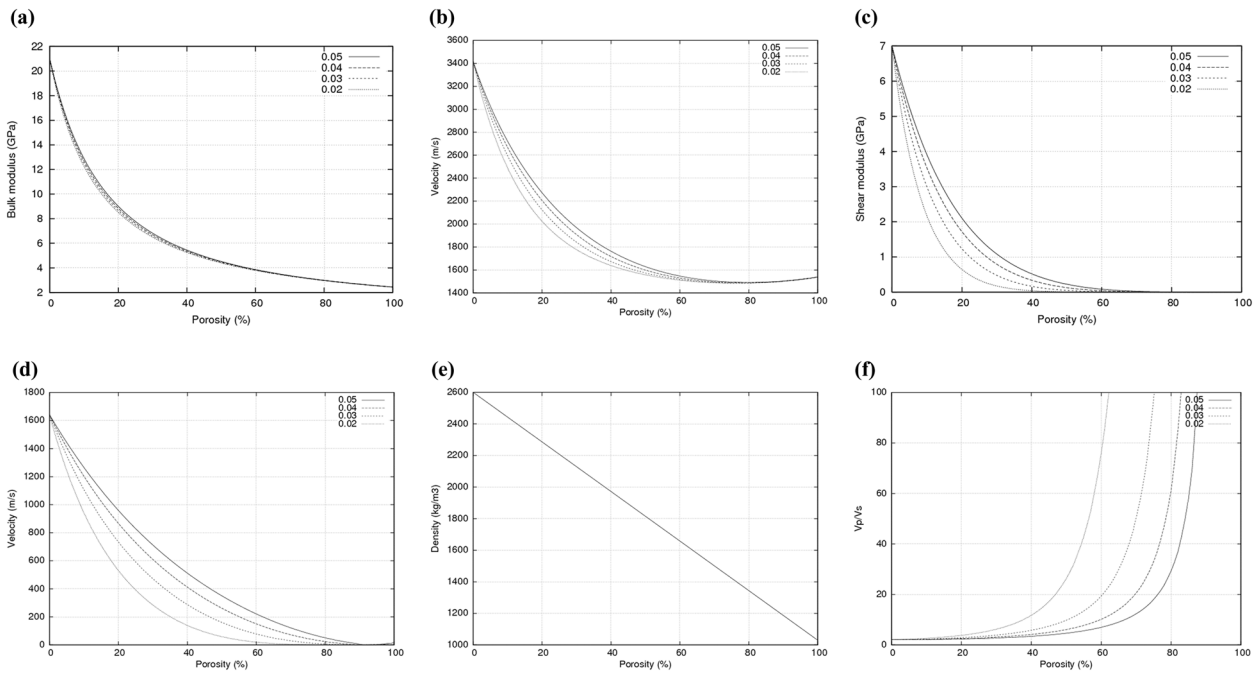

Figure 9 Properties of clay–water mix modelled by four different aspect ratios. a) Bulk modulus, b) P-wave velocity, c) shear modulus, d) S-wave velocity, e) density and f) Vp/Vs-ratio.
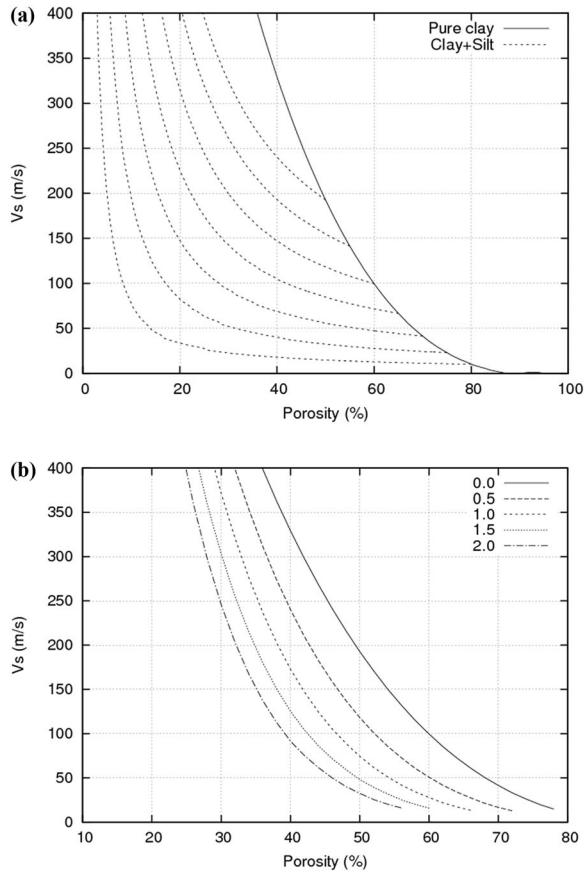
Figure 10 a) shows how V_s varies with porosity when silt is added to clay with different initial porosities. b) shows how V_s varies with porosity for constant ratios of silt and clay (by changing the water content). The solid line is the same in both figures and represents pure clay (with no silt).

Figure 11 Inverted V_s model (solid line, upper axis) and porosity (dashed line, lower axis) deduced from V_s by assuming a silt–clay ratio of 1.0. The porosities are plotted at the mid-point of each layer.

data. Figure 10 shows modelled S-wave velocities as function of water-filled porosity for various clay-to-silt fractions, and where the silt-to-water fractions alter at which silt grains are included. Figures 9 and 10 show in particular two prominent features: First, the V_p/V_s ratios are orders of magnitude higher than those of more compacted sediments. Second, for the same porosity, the S-wave velocity decreases with increased silt-to-clay fraction. The reason for the latter is that, in order to maintain the porosity, the water-filled porosity of the clay needs to increase when porous clay is replaced by silt grains, which have no porosity. The S-wave velocity modelling is consistent with data of Ayres and Theilen (1999) who studied mechanical properties of seabed samples from the Barents Sea, and Rodrigues-Suarez and Stewart (2000) who undertook direct S-wave velocity measurements of the upper 130 m of seabed 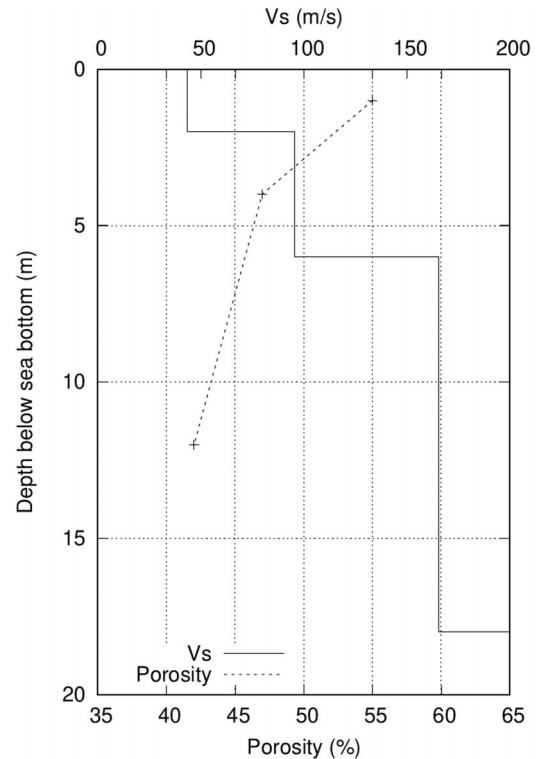sediments outside Brazil. The modelled S-wave velocities versus porosity curves in Figure 10 now facilitate to predict the porosities of the upper sediments using the S-wave velocities inverted from the Scholte waves. The porosity estimates will thus depend on the silt-to-clay fraction. Figure 11 shows the porosity versus depth profile inferred from the S-wave velocity for a silt-to-clay fraction of 1.

DISCUSSION

An objective of this study has been to emphasize how to acquire Scholte wave data during seismic surveying on floating ice on shallow water. The velocity dispersion of Scholte waves can provide information of the near-surface sediments in the transition from land to sea in Arctic regions. Our analyses indicate that Scholte waves can be recorded when both the source and geophone receivers are located on the ice surface, but that they will be difficult to observe due to the flexural waves. The use of air guns below the ice improves the signal-to-noise ratio, especially if the air guns are lowered to more than 3 m below the ice in order to reduce the impact of ice flexural waves. Vertical geophones on the ice are more efficient than hydrophones just below the ice.

The Scholte waves were observed only in a very narrow frequency interval. This together with the smooth character of the obtained phase and group velocity curves suggest that the information content of these curves are very limited and that only a few observation points are necessary to contain the available information. The uncertainties in the observations depend on how accurate one can read the phase velocity gathers (see Fig. 6), which is a somewhat subjective matter. In the inversion program, the uncertainties were set to 8 m/s for phase velocities and 5 m/s for group velocities. However, the program does not compute uncertainties in the model parameters, and a few experiments suggest that the results depended only on the ratio between the phase and the group velocity uncertainties. The program does not allow inversion for layer thicknesses. In order to get an impression of the model uncertainty, one can vary the number and thicknesses of the layers. We found that three sediment layers above the basement were sufficient to fit the data to the modelled curves to within the uncertainties in the observations. The model should not be understood as layers with discontinuities in the velocity, but rather as a coarse representation of the general trend of increasing S-wave velocity with depth in the sediments.

Inversion of Scholte wave data provided S-wave velocities of the seabed sediments. The estimated V_p/V_s ratios are orders of magnitude higher than usually encountered in seismic analysis. This is evidence of very loose sediments and consistent with other studies (Ayres and Theilen 1999; Rodrigues-Suarez and Stewart 2000). Considering the sediments made up of silt, clay and water, a two-step DEM model was used to convert inverted S-wave velocities to porosity data. The rock physics model adapted to the general properties of such loose sediments well, but the accuracy of the estimated porosities could not be evaluated due to lack of direct measurements. An obvious calibration parameter in the rock physics modelling is the clay–water fraction used as a background model for computing the effect of silt. Other parameters to calibrate are the aspect ratio used for mixing clay and water and the elastic properties of clay. The principles of the rock physics model also apply to loose sand–water composites by increasing the aspect ratio of the grains so they become more spherical and the water inclusions to occur as more void-like pores.

CONCLUSIONS

Seismic surveying on floating ice on shallow water shows prominent Scholte wave data, which can be used to map near-surface sediments from land to sea in coastal regions of the Arctic. Air guns below floating ice give stronger signal-to-noise ratio than explosives fired on top of the ice. Air guns should be lowered to more than 3 m below the ice to reduce the extent of ice flexural waves. Vertical geophones are in general sensitive to recording of Scholte waves. When hydrophones are used their vertical positioning should be evaluated with respect to the skin depth which depends on the dominant frequency of the Scholte wave data and the corresponding phase velocity. Seabed sediments are generally very loose with very high P-wave to S-wave velocity ratio. A two-step elastic effective medium model can be tuned to quantitatively describe seismic properties of loose sediments, which in turn potentially enables the use of Scholte-wave data for quantitative characterization of seabed properties.

ORCID

Tor Arne Johansen
https://orcid.org/0000-0002-3974-1362
Bent Ole Ruud https://orcid.org/0000-0002-6813-9215

REFERENCES

Aki K. and Richards P.G. 1980. *Quantitative Seismology*, Vol. I and II. Freeman, San Francisco, CA.

Andersen C.F. and Johansen T.A. 2010. Test of rock physics models for prediction of seismic velocities in shallow unconsolidated sands: a well log data case. *Geophysical Prospecting* **58**, 1083–1098.

Avseth P., Mukerji T. and Mavko G. 2005. *Quantitative Seismic interpretation: Applying Rock Physics Tools to Reduce Interpretation Risk*. Cambridge University Press.

Ayres A. and Theilen F. 1999. Relationship between P- and S-wave velocities and geological properties of near-surface sediments of the continental slope of the Barents Sea. *Geophysical Prospecting* **47**, 431–441.

Bachrach R., Dvorkin J. and Nur A. 2000. Seismic velocities and Poisson's ratio of shallow unconsolidated sands. *Geophysics* **65**, 559–564.

Berryman J.G. 1992. Single-scattering approximations for Biot equations of poroelasticity. *Journal of Acoustical Society of America* **91**, 551–571.

Bohlen T., Kugler S., Klein G. and Theilen F. 2004. 1.5D inversion of lateral variation of Scholte-wave dispersion. *Geophysics* **69**, 330–344.

Boiero D., Wiarda E. and Vermeer P. 2013. Surface- and guided-wave inversion for near surface modeling in land and shallow marine seismic data. *The Leading Edge* **32**, 638–645.

De Hoop A.T. and Van der Hilden J.H.M.T., 1983. Generation of acoustic waves by an impulsive line source in a fluid/solid configuration with a plane boundary. *Journal of Acoustical Society of America* **74**, 333–342.

De Hoop A.T. and Van der Hilden J.H.M.T. 1984. Generation of acoustic waves by an impulsive point source in a fluid/solid configuration with a plane boundary. *Journal of Acoustical Society of America* **74**, 1709–1715.

Hald M., Dahlgren T., Olsen T.-E. and Lebesbye E. 2001. Late Holocene palaeoceanography in Van Mijenfjorden, Svalbard. *Polar Research* **20**, 23–35.

Herrmann R.B. 2013. Computer programs in seismology: an evolving tool for instruction and research. *Seismological Research Letters* **84**, 1081–1088.

Johansen T.A., Ruud B.O. and Hope G. 2019a. Seismic on floating ice on shallow water: observations and modeling of guided wave modes. *Geophysics* **84**, P1–P13.

Johansen T.A., Ruud B.O., Tømmerbakke R. and Jensen K. 2019b. Seismic on floating ice: data acquisition versus flexural wave noise. *Geophysical Prospecting* **67**, 532–549.

Kugler S., Bohlen T., Bussat S. and Klein G. 2005. Variability of Scholte-wave dispersion in shallow marine sediments. *Journal of Environmental and Engineering Geophysics* **2**, 203–218.

Kugler S., Bohlen T., Forbriger T., Bussat S. and Klein G. 2007. Scholte-wave tomography for shallow-water marine sediments. *Geophysical Journal International* **168**, 551–570.

Landschulze M. 2018. Seismic wave propagation in floating ice sheets – a comparison of numerical approaches and forward modelling. *Near Surface Geophysics* **16**, 493–505.

Ludwig W.J., Nafe J.E. and Drake C.L. 1970. Seismic refraction, In: *The Sea*, Vol. **4** (ed. A.E. Maxwell), pp. 53–84. Wiley.

Mavko G., Mukerji T. and Dvorkin J. 1998. *The Rock Physics Handbook*. Cambridge University Press.

McMechan G.A. and Yedlin M.J. 1981. Analysis of dispersive waves by wave field transformation. *Geophysics* **46**, 869–874.

Moyano B., Spikes K.T., Johansen T.A. and Mondol N.H. 2012. Modeling compaction effects on elastic properties of clay water composites. *Geophysics* **77**, D171–D183.

Park C.B., Miller R.D. and Xia J. 1998. Imaging dispersion curves of surface waves on multi-channel record. *SEG Technical Program, Expanded Abstracts,* 1377–1380.

Park C.B., Miller R.D., Xia J., Ivanov J., Sonnichsen G.V., Hunter J.A., *et al*. 2005. Underwater MASW to evaluate stiffness of water-bottom sediments. *The Leading Edge* **24**, 724–728.

Rodrigues-Suarez C. and Stewart R.R. 2000. Shear-wave velocities in shallow marine sediments. SEG 2000 Expanded Abstracts.

Schmidt H. 2011. OASES Version 3.1 user guide and reference manual. Retrieved from: http://lamss.mit.edu/lamss/pmwiki/pmwiki.php?n=Site.Oases

Schmidt H. and Tango G. 1986. Efficient global matrix approach to the computation of synthetic seismograms. *Geophysical Journal of Royal Astronomical Society* **84**, 331–359.

Vardy M.E., Vanneste M., Henstock T.J., Clare M.A., Forsberg C.F. and Provenzano G. 2017. State-of-the-art remote characterization of shallow marine sediments: the road to a fully integrated solution. *Near Surface Geophysics* **15**, 387–402.

Vinh P.C. 2013. Scholte wave velocity formulae. *Wave Motion* **50**, 180–190.

Walton K. 1987. The effective elastic moduli of a random packing of spheres. *Journal of the Mechanics and Physics of Solids* **35**, 213–226.

Wood A.W. 1955. *A Textbook of Sound*. The MacMillan Co.

Zheng Y., Fang X., Liu J. and Fehler M.C. 2012. Scholte waves generated by seafloor topography. Lab Report, MIT.

Zimmer M., Prasad M., Mavko G. and Nur A. 2007a. Seismic velocities of unconsolidated sands: part 1 – pressure trends from 0.1 to 20 MPa. *Geophysics* **72**, E1–E13.

Zimmer M., Prasad M., Mavko G. and Nur A. 2007b. Seismic Velocities of unconsolidated sands: part 2 – influence of sorting- and compaction-induced porosity variation. *Geophysics* **72**, E15–E25.